

Cavity-induced topological edge and corner states

Motohiko Ezawa¹

¹*Department of Applied Physics, University of Tokyo, Hongo 7-3-1, 113-8656, Japan*

We investigate a two-level system with alternating XX coupling in a photon cavity. It is mapped to a free boson model equally coupled to a photon, whose interaction is highly nonlocal. Some intriguing topological phenomena emerge as a function of the photon coupling. The photon energy level anticrosses the zero-energy topological edges at a certain photon coupling, around which the symmetric edge state acquires nonzero energy due to the mixing with the photon. Furthermore, the photon state is transformed into the topological zero-energy edge or corner state when the photon coupling is strong enough. It is a cavity-induced topological edge or corner state. On the other hand, the other topological edge or corner states do not couple with the photon and remains at zero energy even in the presence of the cavity. We analyze a cavity-induced topological edge state in the Su-Schrieffer-Heeger model and a cavity-induced topological corner state in the breathing Kagome model.

Introduction: Cavity quantum-electrodynamics (QED) is a field of studying the coupling effect between atoms with discrete levels and a photon[1–5]. For example, by placing two mirrors in parallel, the energy of photon is quantized and cavity QED is realized. Cavity QED is also realized in superconducting qubits based on Josephson junctions[6, 7]. The coupling constant between the discrete levels and a photon is largely enhanced experimentally[8–12].

Recently, cavity quantum materials attract much attention[13], where a material instead of an atom is deposited in the mirrors. Superconductivity[14], ferroelectricity[15], photon-magnon coupling[38] and quantum Hall effects[16–18] are studied in the context of cavity quantum materials. A fermionic Su-Schrieffer-Heeger (SSH) model coupled with a photon is studied[19–22]. Topological properties of interacting atoms in the cavity are also discussed[23–27], where superconducting qubits enable us to realize strong inter-atomic couplings[24, 25].

In this paper, we investigate the topological zero-energy edge and corner states in cavity-coupled arrays of an interacting two-level system. It is mapped to a hopping model with an additional site representing a photon, which coupled to all of the other sites equally. We analyze a dimerized one-dimensional chain and a breathing Kagome model with alternating XX interactions. We show that they are mapped to the SSH model and the breathing Kagome second-order topological insulator model coupled with an additional photon site, respectively. Intriguing phenomena occur on the photon state and a topological edge or corner state. As the coupling with the cavity increases, the photon state is smoothly transformed into the symmetric edge state or the C_3 -symmetric corner state, while the latter edge state or corner state is smoothly transformed into the photon state. We call it the cavity-induced edge or corner state. On the other hand, the other topological edge state and corner states remain as they are because they do not couple with the photon.

Cavity pseudospin system: Cavity QED with the XX interaction is described by

$$H = \hbar\omega_0 \hat{a}^\dagger \hat{a} + H_{\text{spin}} + \hbar g \sum_{\alpha} (\hat{a}^\dagger \sigma_{\alpha}^{-} + \hat{a} \sigma_{\alpha}^{+}), \quad (1)$$

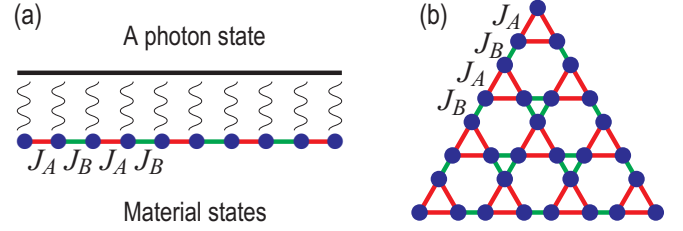


FIG. 1. (a) Illustration of the SSH model with each site equally coupled with a single photon. (b) That of the breathing Kagome lattice.

together with the pseudospin Hamiltonian

$$H_{\text{spin}} = \hbar\omega_s \left(\sum_{\alpha} \frac{\sigma_{\alpha}^{+} \sigma_{\alpha}^{-}}{2} - 1 \right) - \sum_{\alpha, \beta} J_{\alpha\beta} (\sigma_{\alpha}^{-} \sigma_{\beta}^{+} + \sigma_{\alpha}^{+} \sigma_{\beta}^{-}), \quad (2)$$

where α and β are the indices of atoms, σ is a pseudospin operator describing the two levels of the atom, and $J_{\alpha\beta}$ is the exchange coupling constant. We take $0 < \omega_0 < \omega_s$ and have subtracted the energy of the single spin $\hbar\omega_s$ in (2). The Hamiltonian (1) is called the Jaynes-Cummings model[28] without the exchange interaction terms ($J_{\alpha\beta} = 0$). The exchange interaction terms are realized based on superconducting qubits[24, 25].

There is a conserved quantity $[H, N] = 0$ with the total number $N = \hat{a}^\dagger \hat{a} + \sum_{\alpha} \sigma_{\alpha}^{+} \sigma_{\alpha}^{-}$. We consider the case $N = 1$. In this case, the system (1) together with (2) is equivalently described by the bosonic Hamiltonian

$$H_{\text{boson}} = - \sum_{\alpha, \beta} J_{\alpha\beta} (\hat{b}_{\alpha}^{\dagger} \hat{b}_{\beta} + \hat{b}_{\beta}^{\dagger} \hat{b}_{\alpha}) + \sum_{\alpha} \hbar\omega_s \hat{b}_{\alpha}^{\dagger} \hat{b}_{\alpha} + \hbar g \sum_{\alpha} (\hat{a}^{\dagger} \hat{b}_{\alpha} + \hat{b}_{\alpha}^{\dagger} \hat{a}) + \hbar\omega_0 \hat{a}^{\dagger} \hat{a} - \hbar\omega_s, \quad (3)$$

where the use is made of the relations[29, 30], $\sigma_{\alpha}^{-} \sigma_{\beta}^{+} = \hat{b}_{\beta}^{\dagger} \hat{b}_{\alpha}$, $\sigma_{\alpha}^{+} \sigma_{\beta}^{-} = \hat{b}_{\alpha}^{\dagger} \hat{b}_{\beta}$, $\hat{a}^{\dagger} \sigma_{\alpha}^{-} = \hat{a}^{\dagger} \hat{b}_{\alpha}$ and $\hat{a} \sigma_{\alpha}^{+} = \hat{b}_{\alpha}^{\dagger} \hat{a}$. The photon couples equally with each atom with the coupling strength $\hbar g$ in (3), which implies that the additional coupling due to the photon is highly nonlocal. Hence, it is a nontrivial problem whether topological properties keep to hold in the presence of the coupling with a photon.

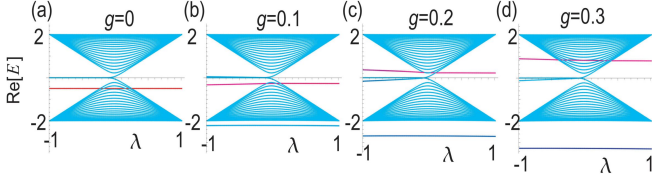


FIG. 2. Energy spectrum as a function of λ , describing bulk bands in cyan, the topological edges in cyan and the photon in red. (a) $\hbar g/J = 0$, (b) $\hbar g/J = 0.1$, (c) $\hbar g/J = 0.2$ and (d) $\hbar g/J = 0.3$. The vertical axis is the energy in units of J . We have set $N = 80$.

Cavity-coupled SSH model: By setting $J_{\alpha\beta} = J_A$ or J_B alternatively in a one-dimensional chain as in Fig.1(a), we obtain the dimerized XX model[31–33],

$$H_{\text{spin-SSH}} = - \sum_{\alpha} [J_A (\sigma_{2\alpha-1}^- \sigma_{2\alpha}^+ + \sigma_{2\alpha-1}^+ \sigma_{2\alpha}^-) + J_B (\sigma_{2\alpha}^- \sigma_{2\alpha+1}^+ + \sigma_{2\alpha}^+ \sigma_{2\alpha+1}^-)] + \hbar\omega_s \left(\sum_{\alpha} \frac{\sigma_{\alpha}^+ \sigma_{\alpha}^-}{2} - 1 \right), \quad (4)$$

from the interaction part of the Hamiltonian (2). The corresponding bosonic Hamiltonian together with the photon coupling and the photon loss reads

$$H_{\text{cavity-SSH}} = \hbar\omega_0 \hat{a}^\dagger \hat{a} - \sum_{\alpha} [J_A (\hat{b}_{2\alpha-1}^\dagger \hat{b}_{2\alpha} + \hat{b}_{2\alpha}^\dagger \hat{b}_{2\alpha-1}) + J_B (\hat{b}_{2\alpha}^\dagger \hat{b}_{2\alpha+1} + \hat{b}_{2\alpha+1}^\dagger \hat{b}_{2\alpha})] - \hbar\omega_s + \hbar g \sum_{\alpha} (\hat{a}^\dagger \hat{b}_{\alpha} + \hat{b}_{\alpha}^\dagger \hat{a}) - \frac{i\hbar}{2} \gamma \hat{a}^\dagger \hat{a}. \quad (5)$$

This is the basic Hamiltonian we analyze. See Eq.(S4) in Supplemental Material with respect to the photon loss term $-\frac{i}{2}\hbar\gamma\hat{a}^\dagger\hat{a}$. We set $J_A = J(1 + \lambda)$ and $J_B = J(1 - \lambda)$ with λ the dimerization. We take $\hbar\gamma/J = 0.2$ in numerical simulations throughout the paper.

In the absence of the photon coupling ($g = 0$), the Hamiltonian matrix is identical to the SSH model. The system is trivial for $|J_A| > |J_B|$ ($\lambda > 0$) and topological for $|J_A| < |J_B|$ ($\lambda < 0$). We show the energy spectrum for $g = 0$ as a function of λ in Fig.2(a). In the trivial phase ($\lambda > 0$), there is no zero-energy edge state. In the topological phase ($\lambda < 0$), there are two zero-energy edge states localized at the left and right edges. They form the symmetric state and the antisymmetric state. The photon state is present as indicated by a red line parallel to the λ -axis.

The energy spectrum is given for $g \neq 0$ as a function of λ in Fig.2(b)~(d). For $\lambda < 0$, the symmetric topological edge state slightly acquires a nonzero energy due to the photon coupling, while the antisymmetric topological edge state remains precisely at zero energy because the antisymmetric state does not couple with the photon. Furthermore, for all λ , one flat state is detached from the bulk band, which we call the detached state. The photon couples only with the symmetric bulk state in the Hamiltonian (5). In addition, the photon state

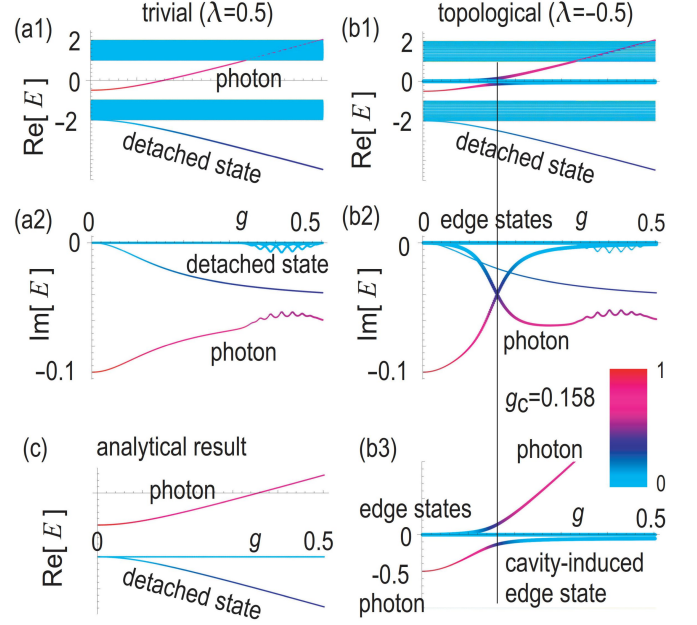


FIG. 3. Energy spectrum as a function of the coupling strength g in the trivial phase with $\lambda = 0.5$ for (a1)~(a2) and in the topological phase with $\lambda = -0.5$ for (b1)~(b3). The photon energy is taken so that $\hbar(\omega_0 - \omega_s) = -0.5J$. Color palette shows the portion of the photon amplitude $\langle \hat{a}^\dagger \hat{a} \rangle$, where red and cyan indicate that it is $\langle \hat{a}^\dagger \hat{a} \rangle = 1$ and $\langle \hat{a}^\dagger \hat{a} \rangle = 0$, respectively. (b3) A detailed band structure at the anticrossing point in the topological phase, where there are three branches, the positive-energy branch, the zero-energy branch and the negative-energy branch. The vertical axis is the energy in units of J . We have set $N = 80$. (c) Analytical result of Eq.(6).

is present as indicated by a red line tilted slightly against the λ -axis.

In order to make clear these properties, we show the energy spectrum as a function of the coupling constant g in Fig.3. For definiteness, we take the energy $\hbar(\omega_0 - \omega_s)$ in the gap between the two bulk bands as in Fig.3(a1). We obtain similar results for other cases of the photon energy, about which we show in Supplemental Material: See Fig.(S1).

We first examine the trivial phase, where the spectrum consists four parts, one photon state, two bulk bands and one detached state. See Fig.3(a1) and (a2). See Fig.4(a) for the distribution of the real part $\text{Re}[\psi_\alpha]$ of the eigenfunction of the detached state, showing that it is almost flat bulk state. The energy of the photon state increases monotonously, while the energy of the detached state decreases monotonously. We make an analytical study of the spectrum of the detached state and the photon state later in the paragraph containing Eq.(6).

Intriguing phenomena emerge in the topological phase, where the photon couples with the symmetric zero-energy edge state as in Fig.3(b1)~(b3). A critical coupling g_c emerges at which an anticrossing of these two states occurs.

We identify the anticrossing point g_c in the real energy spectrum [Fig.3(b1)] from the crossing point in the imaginary energy spectrum [Fig.3(b2)]. A detailed structure of the anticrossing is shown in Fig.3(b3), where we observe three

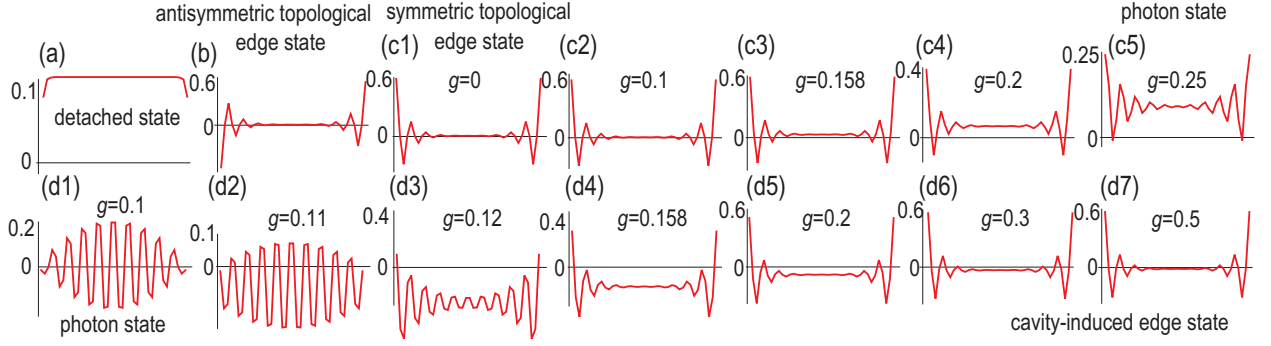


FIG. 4. (a) Real part $\text{Re}[\psi_\alpha]$ of the eigenfunction of the detached state. (b) Those of the antisymmetric topological edge states at zero energy irrespective of g . (c1)~(c5) Those of the negative-energy branch for various g . (d1)~(d7) Those of the positive-energy branch for various g . The horizontal axis is the site index. We have considered the topological phase ($\lambda = -0.5$). The anticrossing point is $\hbar g_c/J = 0.158$. We have set $N = 80$.

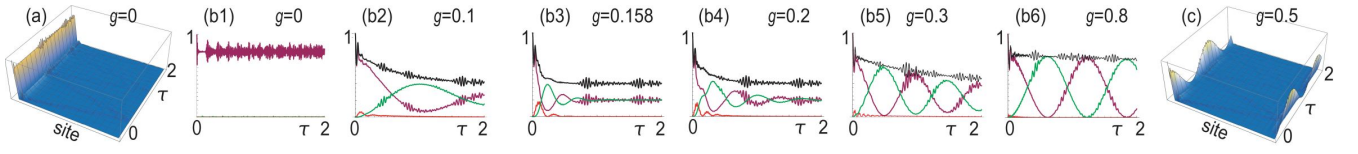


FIG. 5. Quench dynamics of the boson number $\langle \hat{b}_\alpha^\dagger \hat{b}_\alpha \rangle$ starting from the left edge state in the topological phase ($\lambda = -0.5$) for the time period $0 < \tau \equiv tJ/\hbar < 2$, where (a) for $g = 0$ and (c) for $g = 0.5$. (b1)~(b6) Time evolution of the boson number $\langle \hat{b}_1^\dagger \hat{b}_1 \rangle$ at the left edge and $\langle \hat{b}_N^\dagger \hat{b}_N \rangle$ at the right edge and the photon number $\langle \hat{a}^\dagger \hat{a} \rangle$ for the time period $0 < tJ/\hbar < 2$. Violet curves indicate the time evolution of the left-edge site $\langle \hat{b}_1^\dagger \hat{b}_1 \rangle$, green curves indicate the time evolution of the right-edge site $\langle \hat{b}_N^\dagger \hat{b}_N \rangle$, red curves indicate the time evolution of the photon state $\langle \hat{a}^\dagger \hat{a} \rangle$, and black curves indicate the sum of the both-edge sites and the photon state. Only the left edge state is excited for $g = 0$, but both the edges are excited for $g \neq 0$. Out-of-phase oscillations between the left and right edges are suppressed as in (b3) around the anticrossing point $g_c = 0.158$. We have set $N = 80$.

branches, the positive-energy branch, the zero-energy branch and the negative-energy branch.

First, we focus on the positive-energy branch, which starts from the symmetric topological zero-energy edge state at $g = 0$. As g increases, its energy remains almost zero below the anticrossing point ($g < g_c$), but becomes positive for $g > g_c$, as in Fig.3(b1) and (b3). Correspondingly, the edge state is transformed into a bulk state as in Fig.4(c1)~(c5). The symmetric topological zero-energy edge state is transformed eventually into the photon state as g increases.

Second, the zero-energy branch contains only the antisymmetric topological edge state [Fig.4(b)], which is independent of the coupling constant g .

Third, we focus on the negative-energy branch, which starts from a pure photon state at $g = 0$. As g increases, its energy increases toward zero around the anticrossing point g_c , and becomes almost zero for $g > g_c$, as in Fig.3(b1) and (b3). Correspondingly, the bulk state is transformed into the symmetric edge state as in Fig.4(d1)~(d7). The photon state is transformed eventually into the symmetric topological zero-energy edge state as g increases. It is the cavity-induced edge state.

On the other hand, the structures of the two bulk bands is independent of the coupling constant g . In particular, the bulk gap does not close, and hence, the topological properties are robust. We verify this observation by calculating the topological charge in Supplemental Material.

Analytic study: It is intriguing that one bulk state is detached from the bulk band due to the interaction with a photon both in the trivial and topological phases as in Fig.3(a1) and (b1). In order to understanding this phenomenon analytically, we make a study of a simple model with $J_{\alpha\beta} = 0$, where N zero-energy states couple with one photon equally. The energy spectrum is analytically obtained as

$$E/\hbar = \frac{\omega_0 - i\gamma/2 \pm \sqrt{(\omega_0 - i\gamma/2)^2 + 4Ng^2}}{2}, \quad (6)$$

together with $N - 1$ zero-energy level. It is plotted as a function of g in Fig.3. These curves well explain the numerically obtained cavity-induced energy spectrum in Fig.3(a1) and (b1).

Quench dynamics: We study quench dynamics starting from the left-edge site. We numerically solve the Schrödinger equation $i\hbar \frac{d}{dt} |\psi\rangle = H_{\text{cavity-SSH}} |\psi\rangle$ with Eq.(5) by imposing the initial condition $\psi(t=0) = \delta_{\alpha,1}$ on the amplitude.

We show the time evolution in Fig.5. When there is no coupling $g = 0$ as in Fig.5(a) and (b1), only the amplitude at the left edge site is excited. As soon as $g \neq 0$, the right-edge site is also excited via the photon coupling as in Fig.5(b2)~(b6) and (c). The oscillations are out of phase with equal strength between the left and right edges. However, it is notable that the oscillations are suppressed around the anticrossing point g_c as in Fig.5(b3). This is because only the antisymmetric

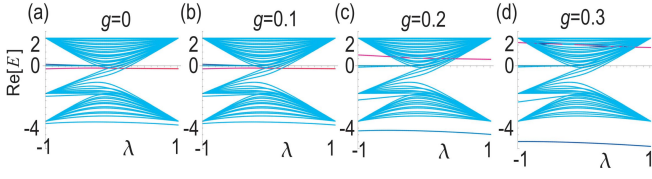


FIG. 6. Energy spectrum as a function of λ in the breathing Kagome model, describing three bulk bands in cyan, the topological corners in cyan and the photon in red. (a) $\hbar g/J = 0$, (b) $\hbar g/J = 0.1$, (c) $\hbar g/J = 0.2$ and (d) $\hbar g/J = 0.3$. The vertical axis is the energy in units of J . We have set $N = 108$.

edge state is at zero energy while the symmetric edge state acquires a non-zero energy.

Cavity-coupled Kagome second-order topological insulator: We next analyze the breathing Kagome XX model as illustrated in Fig.1(b), which is a generalization of the dimerized XX model to the breathing Kagome lattice. The Hamiltonian is given by

$$H_{\text{spin-Kagome}} = - \sum_{\{A,B\}} [J_A (\sigma_A^- \sigma_B^+ + \sigma_A^+ \sigma_B^-) + J_B (\sigma_B^- \sigma_A^+ + \sigma_B^+ \sigma_A^-)] + \hbar \omega_s \left(\sum_{\alpha} \frac{\sigma_{\alpha}^+ \sigma_{\alpha}^-}{2} - 1 \right), \quad (7)$$

where the XX interaction exists in the nearest-neighbor sites in the breathing Kagome lattice. The corresponding Hamiltonian is a second-order topological insulator model[34] with the photon coupling and the photon loss,

$$H_{\text{cavity-Kagome}} = \hbar \omega_0 \hat{a}^\dagger \hat{a} - \sum_{\{A,B\}} [J_A (\hat{b}_A^\dagger \hat{b}_B + \hat{b}_B^\dagger \hat{b}_A) + J_B (\hat{b}_B^\dagger \hat{b}_A + \hat{b}_A^\dagger \hat{b}_B)] + \hbar \omega \hat{b}_\alpha^\dagger \hat{b}_\alpha - \hbar \omega_s + \hbar g \sum_{\alpha} (\hat{a}^\dagger \hat{b}_\alpha + \hat{b}_\alpha^\dagger \hat{a}) - \frac{i\hbar}{2} \gamma \hat{a}^\dagger \hat{a}. \quad (8)$$

This is the basic Hamiltonian.

The analysis is similarly done as in the cavity-coupled SSH model. The system is trivial for $J_A > J_B$ ($\lambda > 0$) and topological for $J_A < J_B$ ($\lambda < 0$). We show the energy spectrum for $g = 0$ as a function of λ in Fig.6(a). In the trivial phase ($\lambda > 0$), there is no zero-energy edge state. In the topological phase ($\lambda < 0$), there are three zero-energy topological corner states localized at the three corners. One of them forms the C_3 symmetric state. In addition, the photon state is present as indicated by a red line parallel to the λ -axis.

The energy spectrum is given for $g \neq 0$ as a function of λ in Fig.6(b)~(d). For $\lambda < 0$, the C_3 symmetric topological corner state slightly acquires a nonzero energy due to the photon coupling, while the other two topological corner states remain at zero energy. Furthermore, for all λ , one flat state is detached from the bulk band, which is the C_3 symmetric bulk state.

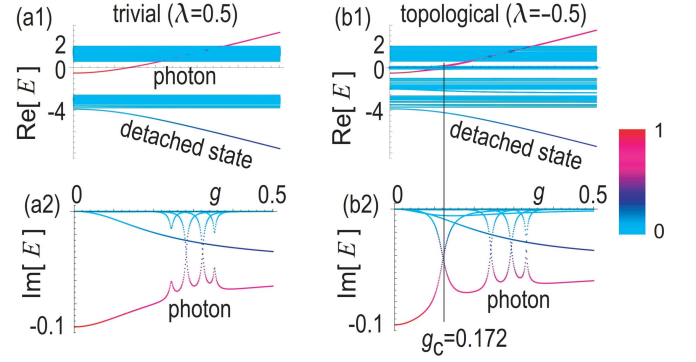


FIG. 7. Energy spectrum of the breathing Kagome model as a function of the coupling strength g in the trivial phase with $\lambda = 0.5$ for (a1)~(a2) and in the topological phase with $\lambda = -0.5$ for (b1)~(b2). The photon energy is taken so that $\hbar(\omega_0 - \omega_s) = 0.5J$. Color palette shows the portion of the photon amplitude $\langle \hat{a}^\dagger \hat{a} \rangle$, where red and cyan indicate that it is $\langle \hat{a}^\dagger \hat{a} \rangle = 1$ and $\langle \hat{a}^\dagger \hat{a} \rangle = 0$, respectively. A detailed band structure at the anticrossing point in the topological phase is almost identical to Fig.3(b3). Only difference is that the zero-energy branch contains two topological corner states except for the C_3 symmetric one. The vertical axis is the energy in units of J . We have set $N = 108$.

We show the energy spectrum as a function of the coupling constant g in Fig.7. For definiteness, we take the photon energy $\hbar(\omega_0 - \omega_s)$ in the gap between the two bulk bands near the zero-energy level as in Fig.7(a1) and (b1). In the trivial phase the spectrum consists four parts, one photon state, two bulk bands and one detached state: See Fig.7(a1) and (a2). The energy of the photon state increases monotonously while the energy of the detached state decreases monotonously.

On the other hand, in the topological phase the photon state anticrosses the C_3 symmetric corner state as in Fig.7(b1). The anticrossing point g_c in the real energy spectrum is identified from the crossing point in the imaginary energy spectrum as in Fig.7(b2). A detailed structure of the anticrossing is very similar to the one in the SSH model shown in Fig.3(b3). We observe three branches, the positive-energy branch, the zero-energy branch and the negative-energy branch. The main difference is that there are two zero-energy corner states in the zero-energy branch. In the positive-energy branch, the C_3 symmetric edge state is transformed eventually into the photon state as g increases. In the negative-energy branch, the photon state is transformed eventually into the C_3 symmetric topological zero-energy edge state as g increases. It is the cavity-induced corner state.

Discussion: The boson numbers $\langle \hat{b}_\alpha^\dagger \hat{b}_\alpha \rangle$ of superconducting qubits are experimentally accessible by quantum non-demolition measurements[35]. On the other hand, the photon number $\langle \hat{a}^\dagger \hat{a} \rangle$ is experimentally observable in superconducting circuits[36]. Another way is the use of magnets, where strong photon-magnon coupling is realized[37–39]. There is a possibility that our system is realized in magnets.

This work is supported by CREST, JST (Grants No. JPMJCR20T2) and Grants-in-Aid for Scientific Research from MEXT KAKENHI (Grant No. 23H00171).

-
- [1] T. Pellizzari, S. A. Gardiner, J. I. Cirac, and P. Zoller, Decoherence, Continuous Observation, and Quantum Computing: A Cavity QED Model, *Phys. Rev. Lett.* 75, 3788 (1995).
- [2] A. Imamoglu, D. D. Awschalom, G. Burkard, D. P. DiVincenzo, D. Loss, M. Sherwin, and A. Small Quantum information processing using quantum dot spins and cavity QED, *Phys. Rev. Lett.* 83, 4204 (1999).
- [3] J. Ye, D. W. Vernooy, and H. J. Kimble, Trapping of Single Atoms in Cavity QED, *Phys. Rev. Lett.* 83, 4987 (1999).
- [4] Shi-Biao Zheng and Guang-Can Guo, Efficient Scheme for Two-Atom Entanglement and Quantum Information Processing in Cavity QED, *Phys. Rev. Lett.* 85, 2392 (2000).
- [5] Alexandre Blais, Ren-Shou Huang, Andreas Wallraff, S. M. Girvin, and R. J. Schoelkopf, Cavity quantum electrodynamics for superconducting electrical circuits: An architecture for quantum computation, *Phys. Rev. A* 69, 062320 (2004).
- [6] Xiu Gu, Anton Frisk Kockum, Adam Miranowicz, Yu-xi Liu and Franco Nori, Microwave photonics with superconducting quantum circuits, *Physics Reports* 718, 1 (2017).
- [7] Alexandre Blais, Arne L. Grimsmo, S. M. Girvin, Andreas Wallraff, *Circuit Quantum Electrodynamics*, *Rev. Mod. Phys.* 93, 25005 (2021).
- [8] J. Bourassa, J. M. Gambetta, A. A. Abdumalikov, Jr., O. Astafiev, Y. Nakamura, and A. Blais, Ultrastrong coupling regime of cavity QED with phase-biased flux qubits, *Phys. Rev. A* 80, 032109 (2009).
- [9] T. Niemczyk, F. Deppe, H. Huebl, E. P. Menzel, F. Hocke, M. J. Schwarz, J. J. Garcia-Ripoll, D. Zueco, T. Hummer, E. Solano, A. Marx and R. Gross, Circuit quantum electrodynamics in the ultrastrong-coupling regime, *Nature Physics* volume 6, 772 (2010).
- [10] Anton Frisk Kockum, Adam Miranowicz, Simone De Liberato, Salvatore Savasta and Franco Nori, Ultrastrong coupling between light and matter, *Nature Reviews Physics* 1, 19 (2019).
- [11] P. Forn-Diaz, L. Lamata, E. Rico, J. Kono, and E. Solano, Ultrastrong coupling regimes of light-matter interaction, *Rev. Mod. Phys.* 91, 025005 (2019).
- [12] Y. Ashida, A. Imamoglu, and E. Demler, Cavity quantum electrodynamics at arbitrary light-matter coupling strengths, *Phys. Rev. Lett.* 126, 153603 (2021).
- [13] Frank Schlawin, Dante M. Kennes, Michael A. Sentef, *Cavity quantum materials*, *Applied Physics Reviews* 9, 011312 (2022).
- [14] F. Schlawin, A. Cavalleri, and D. Jaksch, Cavity-mediated electron-photon superconductivity, *Phys. Rev. Lett.* 122, 133602 (2019).
- [15] Y. Ashida, A. Imamoglu, J. Faist, D. Jaksch, A. Cavalleri, and E. Demler, Quantum electrodynamic control of matter: Cavity-enhanced ferroelectric phase transition, *Phys. Rev. X* 10, 041027 (2020).
- [16] O. V. Kibis, O. Kyriienko, and I. A. Shelykh, Band gap in graphene induced by vacuum fluctuations, *Phys. Rev. B* 84, 195413 (2011).
- [17] G. Scalari, C. Maissen, D. Turcinkov a, D. Hagenmuller, S. De Liberato, C. Ciuti, C. Reichl, D. Schuh, W. Wegscheider, M. Beck, and J. Faist, Ultrastrong coupling of the cyclotron transition of a 2D electron gas to a THz metamaterial, *Science* 335, 1323 (2012).
- [18] X. Wang, E. Ronca, and M. A. Sentef, Cavity quantum electrodynamical Chern insulator: Towards light-induced quantized anomalous Hall effect in graphene, *Phys. Rev. B* 99, 235156 (2019).
- [19] O. Dmytruk and M. Schirò, Controlling topological phases of matter with quantum light, *Com. Phys* 5, 271 (2022).
- [20] B. Perez-Gonzalez, Gomez-Leon and G. Platero, *Physical Chemistry Chemical Physics* 24, 15860 (2022).
- [21] Da-Wei Wang, Chengsong Zhao, Junya Yang, Ye-Ting Yan, and Ling Zhou, Simulating the extended Su-Schrieffer-Heeger model and transferring an entangled state based on a hybrid cavity-magnon array, *Phys. Rev. A* 107, 053701 (2023).
- [22] D. Shaffer, M. Claassen, A. Srivastava and L. H. Santos, Entanglement and Topology in Su-Schrieffer-Heeger Cavity Quantum Electrodynamics, *arXiv:2308.08588*
- [23] C. A. Downing, T. J. Sturges, G. Weick, M. Stobińska, L. Martin Moreno, Topological phases of polaritons in a cavity waveguide, *Phys. Rev. Lett.* 123, 217401 (2019).
- [24] W. Nie, Z. H. Peng, F. Nori, and Y. X. Liu, Topologically Protected Quantum Coherence in a Superatom, *Phys. Rev. Lett.* 124(2), 023603 (2020).
- [25] W. Nie and Y.-X. Liu, Bandgap-assisted quantum control of topological edge states in a cavity, *Phys. Rev. Res.* 2(1), 012076(R) (2020).
- [26] Chen-yang Wang, Yun-jie Zheng, Mei-song Wei, Ming-jie Liao, Zi-jian Lin, Ce Wang, Ya-ping Yang, and Jing-ping Xu, Influence of a topological artificial atom chain on the transmission properties of a cavity *Optics Express* 31, 15342 (2023).
- [27] P. Saugmann and J. Larson, A Fock state lattice approach to quantum optics, *arXiv:2203.13813*
- [28] E. T. Jaynes and F. W. Cummings, Comparison of quantum and semiclassical radiation theories with application to the beam maser, *Proc. IEEE* 51(1), 89–109 (1963).
- [29] H. Bethe, Zur Theorie der Metalle, *Zeitschrift fur Physik* 71 205(1931).
- [30] L. Hulthen, Uber das austauschproblem eines kristalles, *Arkiv for matematik, astronomi och fysik* 26A 1 (1938).
- [31] J. H. Taylor and G. Muller, Magnetic field effects in the dynamics of alternating or anisotropic quantum spin chains, *Physica A: Statistical Mechanics and its Applications* 130, 1 (1985).
- [32] O. Derzhko, T. Krokhnalskii, J. J. Stolze, Dynamic properties of the dimerized spin-isotropic XY chain in a transverse field, *J. Phys. A: Math. Gen.*, 35, 3573 (2002).
- [33] J. Stolze 1, T. Garske, The emptiness formation probability correlation in homogeneous and dimerized XX chains, *Condensed Matter Physics*, 12, 369 (2009).
- [34] M. Ezawa, Higher-Order Topological Insulators and Semimetals on the Breathing Kagome and Pyrochlore Lattices, *Phys. Rev. Lett.* 120, 026801 (2018).
- [35] A. Lupascu, S. Saito, T. Picot, P. C. de Groot, C. J. P. M. Harmans, J. E. Mooij, Quantum non-demolition measurement of a superconducting two-level system, *Nature Physics* 3, 119 (2007).
- [36] D. I. Schuster, A. A. Houck, J. A. Schreier, A. Wallraff, J. M. Gambetta, A. Blais, L. Frunzio, J. Majer, B. Johnson, M. H. Devoret, S. M. Girvin and R. J. Schoelkopf, Resolving photon number states in a superconducting circuit, *Nature* 445, 515 (2007).
- [37] Atac Imamoglu, Cavity QED Based on Collective Magnetic Dipole Coupling: Spin Ensembles as Hybrid Two-Level Systems, *Phys. Rev. Lett.* 102, 083602 (2009).
- [38] O. O. Soykal and M. E. Flatte, Strong field interactions between a nanomagnet and a photonic cavity, *Phys. Rev. Lett.* 104, 077202 (2010).
- [39] Robert Amuss, Christian Koller, Tobias Nauer, Stefan Putz,

Stefan Rotter, Kathrin Sandner, Stephan Schneider, Matthias Schrambock, Georg Steinhauser, Helmut Ritsch, Jorg Schmiedmayer, Johannes Majer, Cavity QED with magnetically coupled collective spin states, Phys. Rev. Lett. 107, 060502 (2011).

Supplemental Material

Cavity-induced topological edge and corner states

Motohiko Ezawa

Department of Applied Physics, The University of Tokyo, 7-3-1 Hongo, Tokyo 113-8656, Japan

I. PHOTON LOSS

Because the cavity is an open quantum system it is necessary to include the effect of the photon loss. The Lindblad equation for the density matrix ρ reads

$$\frac{d\rho}{dt} = -\frac{i}{\hbar} [H, \rho] + \gamma \left(L\rho L^\dagger - \frac{1}{2} \{L^\dagger L, \rho\} \right). \quad (\text{S1})$$

where L is the Lindblad operator describing the dissipation γ . This equation is rewritten in the form of

$$\frac{d\rho}{dt} = -\frac{i}{\hbar} \left(H_{\text{eff}}\rho - \rho H_{\text{eff}}^\dagger \right) + \gamma L\rho L^\dagger, \quad (\text{S2})$$

where H_{eff} is a non-Hermitian effective Hamiltonian defined by

$$H_{\text{eff}} \equiv H - \frac{i\hbar\gamma}{2} L^\dagger L. \quad (\text{S3})$$

The photon loss is described by the Lindblad operator as $L = \hat{a}$. The non-Hermitian effective Hamiltonian reads

$$H_{\text{eff}} \equiv H - \frac{i\hbar}{2} \gamma \hat{a}^\dagger \hat{a}. \quad (\text{S4})$$

The imaginary part of the energy spectrum is proportional to the photon amplitude $\langle \hat{a}^\dagger \hat{a} \rangle$, where the dissipation occurs only in the photon state in the present model.

II. TOPOLOGICAL NUMBER

The Hamiltonian in the momentum space reads

$$\hat{H}(k) = \begin{pmatrix} \hat{b}_A^\dagger & \hat{b}_B^\dagger & \hat{a}^\dagger \end{pmatrix} \begin{pmatrix} 0 & -(J_A + J_B e^{-iak}) & \hbar g \delta(k) \\ -(J_A + J_B e^{-iak}) & 0 & \hbar g \delta(k) \\ \hbar g \delta(k) & \hbar g \delta(k) & \hbar \omega_0 \end{pmatrix} \begin{pmatrix} \hat{b}_A \\ \hat{b}_B \\ \hat{a} \end{pmatrix}. \quad (\text{S5})$$

The winding number for the boson \hat{b}_α is given by

$$W \equiv \frac{1}{2\pi ai} \int_0^{2\pi} \langle \psi_b | \frac{d}{dk} | \psi_b \rangle dk. \quad (\text{S6})$$

where $|\psi_b\rangle$ is the right eigenfunction and $\langle \psi_b |$ is the left eigenfunction of the boson \hat{b}_α . We separate it as

$$W \equiv W_1 + W_2 + W_3, \quad (\text{S7})$$

$$W_1 \equiv \frac{1}{2\pi ai} \lim_{\varepsilon \rightarrow 0} \int_{0+\varepsilon}^{2\pi-\varepsilon} \langle \psi_b | \frac{d}{dk} | \psi_b \rangle dk, \quad (\text{S8})$$

$$W_2 \equiv \frac{1}{2\pi ai} \lim_{\varepsilon \rightarrow 0} \int_0^\varepsilon \langle \psi_b | \frac{d}{dk} | \psi_b \rangle dk, \quad (\text{S9})$$

$$W_3 \equiv \frac{1}{2\pi ai} \lim_{\varepsilon \rightarrow 0} \int_{2\pi-\varepsilon}^{2\pi} \langle \psi_b | \frac{d}{dk} | \psi_b \rangle dk. \quad (\text{S10})$$

W_1 is calculated by using the eigenfunction of the two-band Hamiltonian

$$H(k) = - \begin{pmatrix} 0 & J_A + J_B e^{-iak} \\ J_A + J_B e^{-iak} & 0 \end{pmatrix}, \quad (\text{S11})$$

which is identical to the original SSH model. Eigenenergies are

$$E(k) = \pm \sqrt{J_A^2 + J_B^2 + 2J_A J_B \cos ak}, \quad (\text{S12})$$

and the eigenfunctions are

$$\psi(k) = \frac{1}{\sqrt{2}} \left(1, \mp \frac{J_A + J_B e^{iak}}{|E(k)|} \right). \quad (\text{S13})$$

Hence, we have $W_1 = 1$ for the topological phase ($|J_A| < |J_B|$) and $W_1 = 0$ for the trivial phase ($|J_A| > |J_B|$).

W_2 is rewritten as

$$W_2 \equiv \frac{1}{2\pi a i} \lim_{\varepsilon \rightarrow 0} \varepsilon \langle \psi_b | \psi_b \rangle dk, \quad (\text{S14})$$

where $|\psi_b\rangle$ is the eigenfunction of (S11) and $\langle \psi_b |$ is the eigen function of

$$H(0) = \begin{pmatrix} 0 & -(J_A + J_B) & \hbar g \\ -(J_A + J_B) & 0 & \hbar g \\ \hbar g & \hbar g & \hbar \omega_0 \end{pmatrix}, \quad (\text{S15})$$

where the eigenenergies are

$$E(0) = J_A + J_B, \frac{-(J_A + J_B) + \hbar \omega' \sqrt{(J_A + J_B + \hbar \omega_0)^2 + 8\hbar^2 g^2}}{2}, \quad (\text{S16})$$

and the corresponding eigenfunctions are

$$\psi(0) = \frac{1}{\sqrt{2}} (-1, 1, 0), \frac{1}{\sqrt{1 + 2|f_{\pm}|^2}} (f_{\pm}, f_{\pm}, 1), \quad (\text{S17})$$

with

$$f_{\pm} \equiv \frac{J_A + J_B - \hbar \omega_0 \pm \sqrt{(J_A + J_B - \hbar \omega_0)^2 + 8\hbar^2 g^2}}{4\hbar g}. \quad (\text{S18})$$

We take the part of boson \hat{b} , which is given by

$$\psi(0) = \frac{1}{\sqrt{2}} (1, 1). \quad (\text{S19})$$

We have the finite inner product

$$\lim_{\varepsilon \rightarrow +0} \langle \psi_b(\varepsilon) | \psi_b(0) \rangle = 1, \quad (\text{S20})$$

and hence, we obtain $W_2 = 0$. In the similar way, we have $W_3 = 0$. As a result, we conclude $W = 1$ for the topological phase ($|J_A| < |J_B|$) and $W = 0$ for the trivial phase ($|J_A| > |J_B|$). Hence, there is no topological phase transition induced by the photon coupling.

III. CAVITY-COUPLED SSH MODEL

We investigate the cavity-coupled SSH model. There are three cases with respect to the energy of the photon. (i) It is taken in the gap between the two bulk bands as in Fig.S1(a1). (ii) It is taken within the lower bulk band as in Fig.S1(a2). (iii) It is taken smaller than the lower limit of the lower bulk band as in Fig.S1(a3). We have analyzed the case (i) in the main text. By comparing Fig.S1(a1) and (a2), the case (ii) is essentially the same as the case (i).

There are some different features in the case (iii). However, when we interchange the roles of the photon state and the detached state, all results follows as they are. In the trivial phase, for instance, the energy of the detached state decreases monotonously while the energy of the photon state increases monotonously as in Fig.S1(c3). In the topological phase, the energies of the detached state and the topological zero-energy edge state anticross at g_c . Furthermore, the detached state is transformed into the symmetric topological zero-energy edge state as g increases, and vice versa as in Fig.S1(c3).

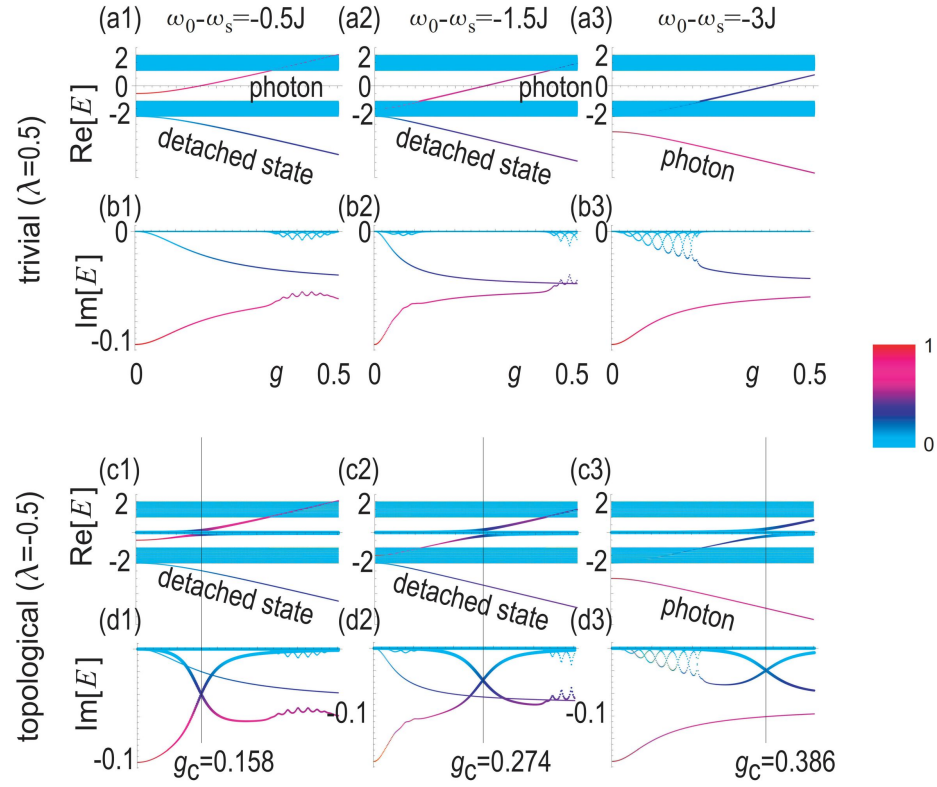


FIG. S1. Energy spectrum as a function of the coupling strength g in the trivial phase with $\lambda = 0.5$ for (a1)~(b3) and in the topological phase with $\lambda = -0.5$ for (c1)~(d3). The photon energy is taken as (*1) $\hbar(\omega_0 - \omega_s) = -0.5J$, (*2) $\hbar(\omega_0 - \omega_s) = -1.5J$ and (*3) $\hbar(\omega_0 - \omega_s) = -3J$. Color palette shows the portion of the photon amplitude $\langle \hat{a}^\dagger \hat{a} \rangle$, where red and cyan indicate that it is $\langle \hat{a}^\dagger \hat{a} \rangle = 1$ and $\langle \hat{a}^\dagger \hat{a} \rangle = 0$, respectively. A detailed band structure at the anticrossing point is shown in Fig.3(b3). The vertical axis is the energy in units of J . We have set $N = 108$.